


Review

Carbon Dioxide Methanation Enabled by Biochar-Nanocatalyst Composite Materials: A Mini-Review

Mengqi Tang¹, Ahmed Gamal², Arvind K. Bhakta^{1,3}, Khoulood Jlassi², Aboubakr M. Abdullah^{2,*} and Mohamed M. Chehimi^{1,*} 

¹ ITODYS Laboratory, Université Paris Cité, CNRS (UMR 7086), F-75013 Paris, France; mengqi.tang@etu.u-paris.fr (M.T.); arvind-kumar.bhakta@u-paris.fr (A.K.B.)

² Center for Advanced Materials, Qatar University, Doha 2713, Qatar; a.mohamad@qu.edu.qa (A.G.); khoulood.jlassi@qu.edu.qa (K.J.)

³ Department of Chemistry, St. Joseph's University, Bangalore 560027, India

* Correspondence: bakr@qu.edu.qa (A.M.A.); mohamed.chehimi@cnrs.fr (M.M.C.)

Abstract: Due to ever-increasing global warming, the scientific community is concerned with finding immediate solutions to reduce or utilize carbon dioxide (CO₂) and convert it in useful compounds. In this context, the reductive process of CO₂ methanation has been well-investigated and found to be attractive due to its simplicity. However, it requires the development of highly active catalysts. In this mini-review, the focus is on biochar-immobilized nanocatalysts for CO₂ methanation. We summarize the recent literature on the topic, reporting strategies for designing biochar with immobilized nanocatalysts and their performance in CO₂ methanation. We review the thermochemical transformation of biomass into biochar and its decoration with CO₂ methanation catalysts. We also tackle direct methods of obtaining biochar nanocatalysts, in one pot, from nanocatalyst precursor-impregnated biomass. We review the effect of the initial biomass nature, as well as the conditions that permit tuning the performances of the composite catalysts. Finally, we discuss the CO₂ methanation performance and how it could be improved, keeping in mind low operation costs and sustainability.

Keywords: carbon dioxide utilization; methanation; reduction of CO₂ emission; biochar; immobilized nanocatalysts



Citation: Tang, M.; Gamal, A.; Bhakta, A.K.; Jlassi, K.; Abdullah, A.M.; Chehimi, M.M. Carbon Dioxide Methanation Enabled by Biochar-Nanocatalyst Composite Materials: A Mini-Review. *Catalysts* **2024**, *14*, 155. <https://doi.org/10.3390/catal14020155>

Academic Editors: Vitali A. Grinberg and Alexander D. Modestov

Received: 15 December 2023

Revised: 9 February 2024

Accepted: 12 February 2024

Published: 19 February 2024

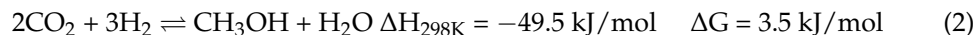
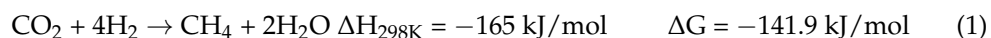


Copyright: © 2024 by the authors. Licensee MDPI, Basel, Switzerland. This article is an open access article distributed under the terms and conditions of the Creative Commons Attribution (CC BY) license (<https://creativecommons.org/licenses/by/4.0/>).

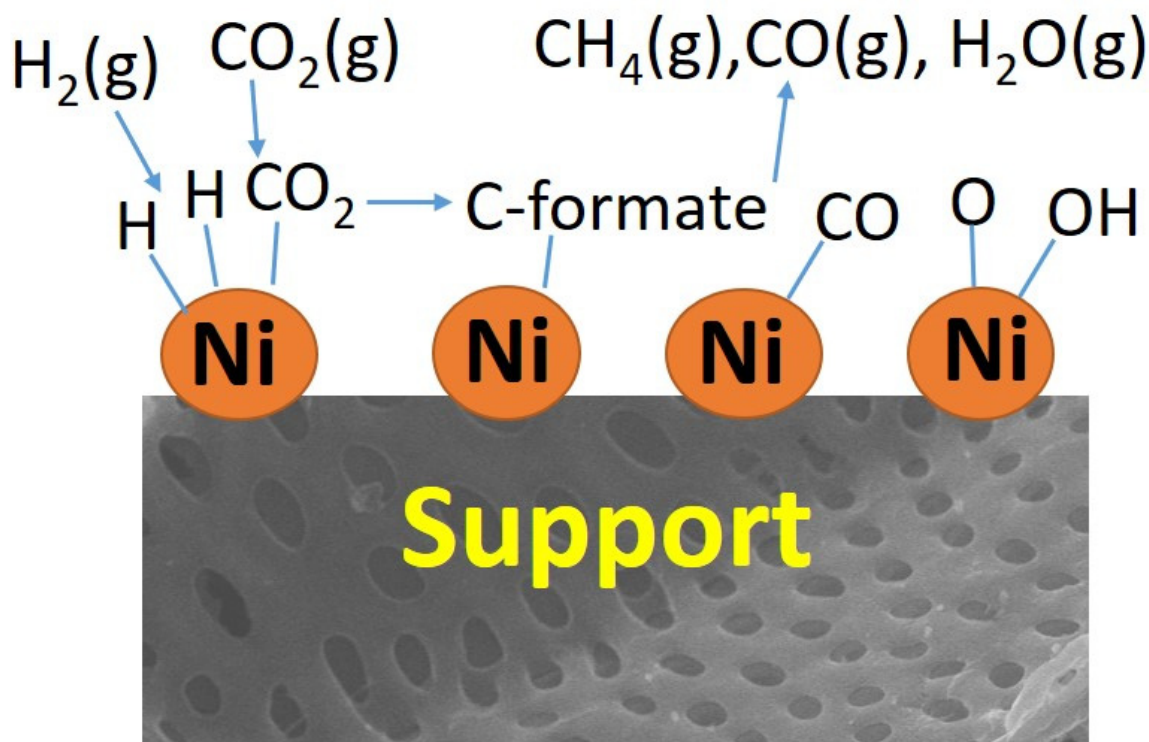
1. Introduction

The inevitable combustion of fossil fuels releases massive amounts of greenhouse gases (GHGs), especially CO₂, which is the leading cause of global warming and climate change [1]. CO₂ alone contributes 20% of the emitted GHGs, which increased by more than 15% in the last decade to reach nearly 30 billion tons, with a high expectation of this number doubling by 2050 [2,3]. Thereby, it is crucial to reduce by 20 gigatons/year the emitted CO₂ within the coming thirty years to become near zero at the end of this century in order to decrease the Earth's temperature to 6 °C [4]. CO₂ mitigation in the atmosphere is investigated via two strategies: capture and utilization. CO₂ can be captured by numerous high surface porous materials [5] or converted into useful compounds and fuels, such as dimethyl carbonate [6], or via dry reforming [7,8], CO₂ hydrogenation to methanol [9], and CO₂ methanation [10]. Dry reforming reactions require high operating temperatures, as CH₄ and CO₂ are thermally stable compounds, in addition to the fast coke formation, as carbon originates from two sources (CH₄ and CO₂), which poisons the catalyst and blocks the reactors [11–13]. In addition, the track of CO₂ hydrogenation to methanol requires severe operating conditions, such as high reaction temperatures and high applied pressures, which results in high operational costs [14].

The hydrogenation of CO₂ to methane (Equation (1)) or to methanol (Equation (2)) represents possible pathways to the utilization of CO₂; however, thermodynamically speaking, more heat is released by CO₂ methanation [15].



A simplified mechanism of CO₂ methanation is displayed in Scheme 1; an example is given for a supported nickel nanocatalyst. However, it should be noted that the mechanisms could be affected by the nature of the support [16].



Scheme 1. The CO₂ methanation process over nickel-based catalysts. Adapted from [16] with permission of Elsevier.

Thus, among the CO₂ applications, the methanation reaction is simple to conduct under mild temperature conditions (in the 200–500 °C range); more importantly, such a reaction can be accomplished at ambient pressure [17]. These salient features of CO₂ methanation make it highly popular; Figure 1 shows the remarkable increase in publications on CO₂ methanation in the last ten years. Yet, CO₂ methanation requires efficient catalysts, and in this regard, mono, bimetallic nanocatalysts and other metal/metal oxide combined catalysts have been employed in the pure form or in the dispersed state. In the latter case, high-surface-area catalyst supports are required, and numerous have been employed, namely silica, zeolite, clay, MOF, and carbon allotropes. However, the emerging high-performance material coined as “biochar” has just started to be investigated as a nanocatalyst support for CO₂ methanation.

Given the skyrocketing number of publications on biochar (about 5000–6000 publications yearly since 2021), it is clear that this support obtained by thermochemical treatment of the biomass, mostly lignocellulosic waste, has much to offer; this is what has attracted our attention. In the past two years, we have spent time and effort on the design of biochar nanocatalysts from various lignocellulosic wastes for the degradation of dyes [18–21] and the elimination of other emerging pollutants. Apart from de-pollution, and investigating green and valuable methods to design biochar-based materials for the energy sector, we

decided to invest time in the attractive and challenging process of CO₂ methanation. It is also important to draw the attention of material scientists and catalysis experts to the growing role of biochar in this area. Although there is abundant literature on the design of hybrid catalysts for CO₂ methanation, our search using the Web of Science returned no specific review focusing on biochar-immobilized nanocatalysts for CO₂ methanation; hence, the motivation for this contribution. Indeed, biochar has high potential in the coming years, as it is converted from trash into valuable, functional material under various temperature (300–1000 °C) and atmosphere conditions (N₂, N₂/H₂, steam, CO₂, etc.) [22]. Moreover, biochar could be efficiently decorated with nanocatalysts in simple ways [23]. The transformation of precursors into nanocatalysts over biochar does not necessarily require “beaker chemistry” as a protocol of biochar post-modification, but wet impregnation followed by pyrolysis could lead to the biochar-supported nanocatalyst in one pot [23,24]. Nanocatalyst-modified biochar has raised immense interest owing to its efficiency to catalyze organic synthesis [25], biofuel production [26], electrochemical processes and energy storage [27], and depollution, to name but a few applications [28]. Given the biodiversity, each region has its own agro-wastes, which can be converted into functional biochar, therefore promoting local/regional engineering and saving costs related to the transport and use of commercially available chemicals for the fabrication of synthetic supports (e.g., mesoporous silica). In this sense, biochar holds promise in terms of sustainable development and the circular economy. As several chemical processes use biochar-supported nanocatalysts, one could anticipate the rapid increase of investigations of their catalytic application to CO₂ methanation.

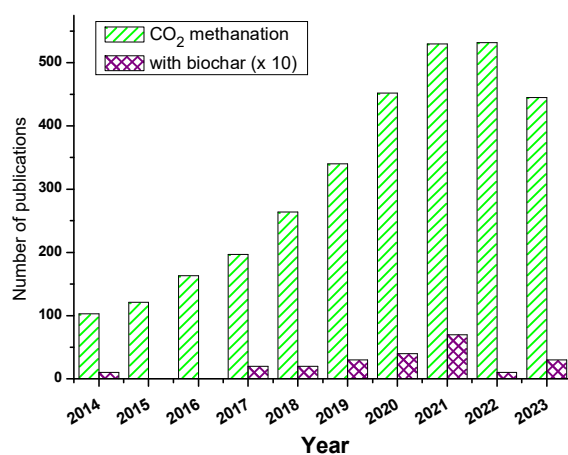


Figure 1. Number of publications per year on CO₂ methanation and the same reaction using biochar materials. Source: Web of Science, last accessed: 17 November 2023.

2. Biochar Catalyst Fabrication and Modification

Biochar serves as an ideal porous support for catalysts prepared by thermochemical methods. Through the various pretreatments or loading of metal nanoparticles to tune its physicochemical properties, the fabrication process results in promising biochar-based composite materials. We present a comprehensive overview of biochar modification, focusing primarily on physical modification, chemical modification, nanoparticle modification, and sequence of wetness impregnation/pyrolysis (Figure 2).

2.1. Biomass Sources

Biochar is a solid product obtained by thermal decomposition of a diverse range of biomass feedstocks in a limited oxygen atmosphere [29]. In order to achieve the goal of biochar production with good physico-chemical properties, as well as reducing waste emissions and increasing by-products during the biochar process, a large number of raw feedstocks are considered, such as forestry residues, animal manure, aquatic plants, municipal waste generated by human activities, factory waste and, particularly, agricultural

lignocellulosic biomass residues [30]. Wan et al. studied the pyrolysis of various biomass feedstocks into biochar; the biomass with higher lignin effectively produced more stable biochar with aromatics [31]. Research by Bhakta et al. [32] showed that different biomasses have different composition, which has a direct effect on the different morphologies of biochar as well as nanoparticle shape and size. Of course, this in turn affects their catalytic properties. For example, when four biomasses, namely sugarcane bagasse (*Saccharum officinarum*), mandarin orange peels (*Citrus reticulata*), China rose petals (*Rosa chinensis*), and algae (*Phaeophyta*), were considered, with the same conditions of impregnation and pyrolysis, the shape and size of ZnO nanoparticles were different. This can be attributed to the different cellulose, hemicellulose, and lignin compositions [32,33]. Also, hydrophobicity, porosity, and hydrophilicity of biomass are important factors.

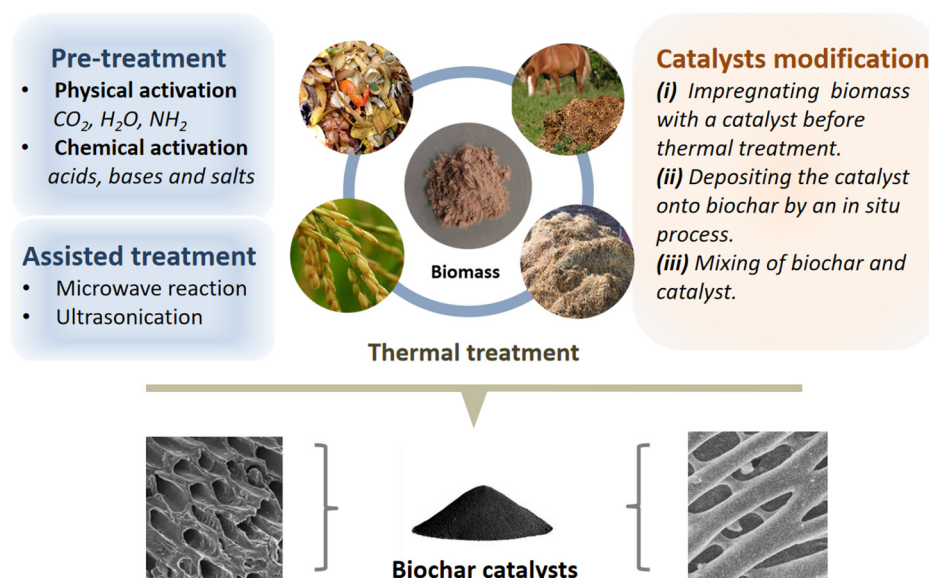


Figure 2. The framework of biochar catalyst preparation via three main methods. The biomass can be pre-treated prior to carbonization. Microwave or ultrasonication can be applied to either the biomass or the obtained biochar.

2.2. Fabrication Process

Thermochemical methods have emerged as a promising technology for the conversion of biomass into valuable products [34]. Herein, the focus is on biomass pyrolysis-derived biochar-immobilized metal catalysts, presenting the carbonaceous materials as a popular topic for environmentally friendly alternatives.

Pyrolysis is a common thermochemical technology; biomass undergoes carbonization in inert or oxygen-limited conditions and is heated above its thermal stability limit without combustion [35,36], resulting in more stable products and solid residues, including large quantities of liquids (bio-oil), solids (biochar), and gases (biosyngas) [37]. Both in fast pyrolysis and flash pyrolysis, biomass is rapidly heated to high temperatures within a short residence time, resulting in dominant yields of oil and gas over charcoal [38,39]. In contrast, slow pyrolysis, characterized by medium–high temperatures (500–900 °C), a slow heating rate (5–10 K/min), and an extended residence time (≥ 10 min), provides an ideal environment and sufficient duration for the production of solid carbonaceous materials, particularly biochar-based materials.

2.3. Precursor Material Pretreatment

Common functional groups attached to the surface of biochar are determined by the raw materials and the pyrolysis conditions. The pretreatment of the biomass with a biochar precursor is a viable strategy to tailor the surface properties of composite catalysts. This section will primarily discuss the impact of physical and chemical pretreatments.

2.3.1. Physical Pretreatment

Physical pretreatment is a pivotal step in enhancing catalyst activity. Most physical activation is performed on the obtained biochar during high-temperature carbonization in an atmosphere of CO_2 , H_2O_2 , NH_2 , or water vapor. Sun et al. [40] proposed a method for the preparation of biochar-based catalysts through CO_2 activation for impedance reduction. They first heated the biochar to a set temperature under an N_2 atmosphere (800–900 °C), and then CO_2 (500 mL/min) was injected to start the activation, which lasted 1 h. The obtained biochar enhanced the graphitization to improve the electron transfer ability.

Iberahim et al. [41] prepared oil palm fiber-activated biochar at 753 °C for 73 min of activation time with 497 mL/min of CO_2 flow. The pH value of the activated biochar was higher than pure biochar and increased as the activation temperature increased from 600 to 800 °C. The catalyst surface pH provides valuable insights into the adsorption of gas molecules, combining consideration of the acidity and basicity of the target gas molecules. As the biochar is activated under a CO_2 atmosphere at high temperatures, this involves oxidative treatment, effectively improving the structural characteristics, which enhances its suitability for applications in catalysis [35].

Feng et al. [42], in their work, described H_2O -activated biochar and ammonia-activated biochar. They used corn straw as raw materials, and activated biochar was prepared by $\text{NH}_3\text{H}_2\text{O}$ activation and H_2O activation to design biochar with hierarchical pore and O/N functional groups. The N-containing functional groups on the ammonia-activated biochar surface had greater adsorption energy for CO_2 and NH_3 than O-containing groups of H_2O activated biochar. This result also highlights the significance of chemical functionalities on the catalyst surface in enhancing performance.

Ultrasonic pretreatment is a physical method that can improve the biochar properties of biochar materials, which contributes to improving the nanoparticle dispersion over biochar composite surfaces without changing the functional structures [43].

2.3.2. Chemical Pretreatment

Chemical pretreatment is another critical precursor material-activated method, involving activators including acids, bases, salts, and more. Based on the literature, employing chemical activation methods for precursor treatment has been shown to develop the catalyst properties, such as surface area, porosity, functional groups, and active sites, in order to increase biochar reaction rates.

Tang et al. [44] used pine nut shells to obtain biochar through KOH pretreatment and calcination methods. Its microporosity was 20 times higher than that of biochar without KOH pretreatment, and its specific surface area was as high as $1850 \text{ m}^2 \cdot \text{g}^{-1}$, which is very suitable for CO_2 adsorption (CO_2 uptake of $6.05 \text{ mmol} \cdot \text{g}^{-1}$ at 1 bar, 273 K).

African almond leaves were first treated with phosphoric acid (H_3PO_4), followed by pyrolysis at high temperatures in an inert environment. Embedding phosphoric acid functional groups (PO_4^{3-}) on the surface through chemical pretreatment increases the adsorption capacity of biochar and can remove >98% of MB dye molecules within 30 min [45]. Nguyen et al. [46] researched the pore-forming effect of ZnCl_2 decomposition during thermal treatment to improve the physicochemical properties of biochar. Biochar derived from brown algal *Ascophyllum nodosum* was synthesized through hydrothermal carbonization (HTC) coupling with ZnCl_2 chemical activation at 700 °C. The activating process with ZnCl_2 changed the pyrolysis path of biochar and improved accessible binding sites, as proved by TG and BET analyses; its acidic and basic groups on the biochar surface were also modified.

2.4. Nanoparticle Loading

Metal loading is a crucial factor influencing the performance of composite catalysts. Biochar materials can be functionalized or modified with the addition of nanoparticles during thermal treatment or physical–chemical reactions, in which the generated composites combine the properties of biochar and nanoparticles. This section will primarily

discuss the impact of different metal loading methods. The relevant literature will be summarized to illustrate the effects of various metal loading strategies on the catalytic activity of composite catalysts.

Snoussi et al. [47] pretreated the biomass by maceration in a hydroalcoholic mixture with ultrasonication assistance and then impregnated it with copper and silver nitrate salts prior to pyrolysis at 500 °C under N₂:H₂ 95%:5% for 1 h, leading to biochar-supported Ag/Cu nanoparticles. Compared to pristine biochar, the biochar made out of the macerated biomass exhibited a noticeable microporosity, with a more accessible and porous structure. N₂-physisorption measurements proved the specific surface area of Ag/Cu-Biochar increased by 20%, and its pore volume was increased 25-fold.

Prabhakaran et al. [48] proposed modification of the surface of biochar by introducing iron oxide nanoparticles and elaborated on the synthesis process of wetness impregnation for 1 h and the hydrothermal method at 180 °C for 12 h to prepare magnetic biochar nanocomposites (Figure 3). The biochar-based iron oxide nanocomposite was ready for reuse after separation and showed a high adsorption capacity for dye removal from aqueous solutions.

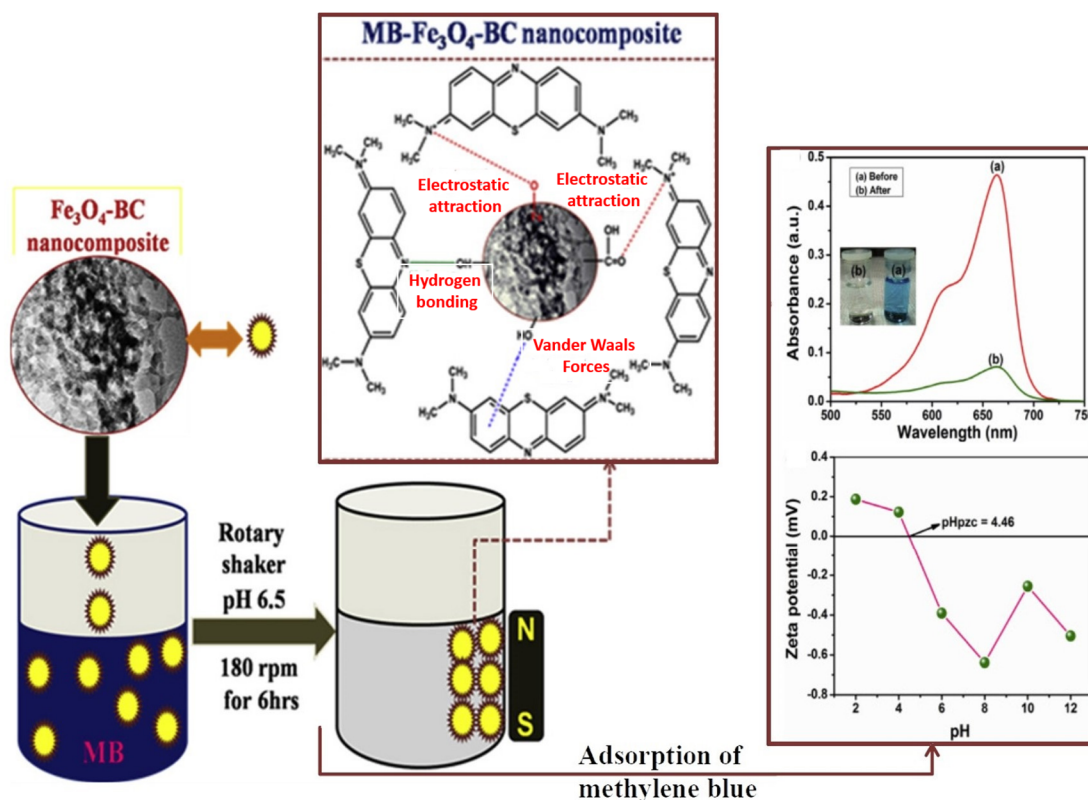


Figure 3. Iron oxygen nanoparticles modified with biochar materials for methylene blue (MB) adsorption. Adapted from [48] with permission of Elsevier.

He et al. [49] prepared bi-nanoparticles that were Co-N loaded onto biochar through a two-step modification method. First, N-doped biochar materials were pretreated and pyrolyzed; then, the Co-N biochar composite materials were synthesized by microwave assistance and pyrolysis again, modifying the Co nanoparticles on the N-doped biochar doped with different nitrogen sources to obtain bi-catalyst biochar composites. Maiti et al. [50] modified highly porous biochar composites with the conductive polymer PANI into binary composites through in situ polymerization for studying the capacitive properties. An activation process with HCl and the oxidizing agent ammonium persulfate (APS) was also applied to increase the energy density and specific capacitance. It follows

that a combination of multiple modifications is necessary to improve biochar, with the desired properties.

2.5. Sequence of Wetness Impregnation/Pyrolysis

The wetness impregnation/pyrolysis method is the most commonly employed technique for the fabrication of biochar composites. This can be achieved either by the modification of biomass before pyrolysis (pre-pyrolysis modification) or by post-pyrolysis modification of biochar. The stepwise loading of bi-catalysts onto biochar follows a similar approach [49]. The order of wet impregnation and pyrolysis significantly influences the physicochemical properties of the biochar composites, such as the pore structure and the specific surface area. SEM analysis indicated that pre-treatment followed by pyrolysis induces the catalyzed carbonization of the biomass and the formation of pores and leads to a considerable surface area [51]. This contrasts with the post-treatment of the pyrolyzed samples, containing less unevenly distributed inorganic particles/larger crystal clusters and resulting in the blocking of pores and reductions in the specific surface area (Figure 4). Wet impregnation modification facilitated the introduction of higher concentrations of metals, leading to the formation of metal oxides on the biochar surface and an improvement in the porous structure. Interestingly, this comparative study of the ecotoxicological characteristics of Zn-decorated biochar prepared by either pretreatment of the biomass or post-treatment of the biochar demonstrated that the final biochar Zn was found to be distinctly different [51]. For example, post-treatment led to biochar Zn with a higher content of polyaromatic hydrocarbons and thus more toxicity. It follows that a comparative study of the method of preparation of reductive composite catalysts could be important when considering CO₂ methanation.

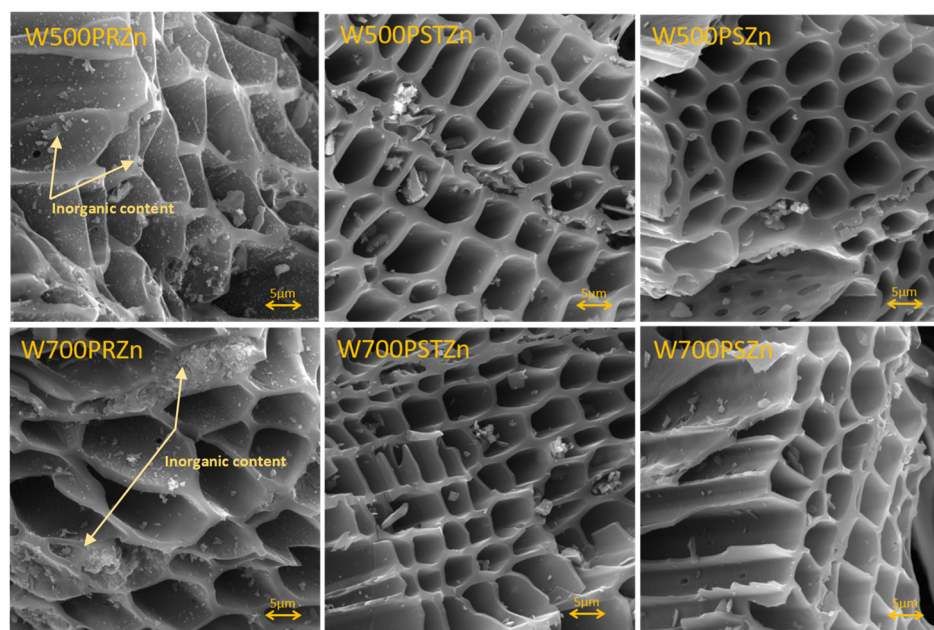


Figure 4. SEM images (5.00 kx magnification) of biochar samples loaded with Zn, prepared under different conditions. Reproduced from [51] with permission of Elsevier. PR: pretreatment; PS: post-treatment; PST: additional pyrolysis step. The numbers 500 and 700 represent the pyrolysis temperatures.

In recent studies, some authors [21,47] reported the synthesis of biochar/bimetallic nanocatalyst composites through mixing biomass into two metal nitrate solutions via a wet impregnation method followed by pyrolysis. SEM results revealed a spacious, porous structure, with metal nanoparticles uniformly dispersed on the surface. XRD analysis

confirmed the presence of a bimetallic alloy, verifying the successful loading of metal nanoparticles onto the biochar substrate.

2.6. Porous Properties of Biochar-Supported Materials

Biochar, derived from biomass conversion under oxygen-free conditions through pyrolysis, significantly influences the porous properties of biochar supports. Table 1 presents the compression pore properties between different biochar-based materials, including their modified biochar and composite materials, considering the impact of preparation methods on the morphological features of the biochar. It is notable that the biochar-based materials offer larger specific surface areas and enriched pore structures. When biomass undergoes pyrolysis, the water loss and volatile components released during the treatment process contribute to the formation of the biochar pore structure and the development of primary pores [52,53].

Table 1. Comparison of porous properties of biochar-supported materials derived different biomass.

Biomass	Samples	Synthesis Methods	Surface Area (m ² /g)	Total Pore (cm ³ /g)	Ref.
White tea waste	Fe ₃ O ₄ /BC	Pyrolysis and co-precipitation	52.2	0.118	[54]
	BC	Pyrolysis	36.6	0.0123	
	White tea waste	Biomass without any treatment	0.196	0.0006	
soybean protein	Activated BC	pre-carbonization and KOH activation	2788	1.65	[55]
	BC	pyrolysis	145	0.073	
Peanut shell	SO ₃ H modified biochar-supported MnO ₂	Sulfuric acid pretreatment, pyrolysis, and co-precipitation for loading MnO ₂	52.27	0.56	[56]
	SO ₃ H modified biochar	Sulfuric acid pretreatment and pyrolysis	83.39	0.10	
	Biochar	pyrolysis	32.27	0.03	
Corn-cob-to-xylose residue	BC/MgO	Impregnation and pyrolysis	407.7	-	[57]
	BC	pyrolysis	232.9	-	
Rubber seed shell	MgAl/LDH-BC	Impregnation and pyrolysis	132.40	0.0732	[58]
	BC	pyrolysis	114.32	0.0617	
Rice husks	BPC/nano zero-valent iron	liquid-phase reduction of BPC	1430.37	1.303	[59]
	BPC	KOH activation and pyrolysis	1503.65	1.315	
	BC/nano zero-valent iron	liquid-phase reduction of BC	574.64	0.370	
	BC	Pyrolysis	420.61	0.310	
Balsa wood powder	MBC Cu ₂ O	Impregnation of MBC	30.3436	0.070830	[60]
	MBC	KOH activation and pyrolysis	837.6070	0.430967	
	BC	pyrolysis	492.2085	0.206011	
	Cu ₂ O	-	15.7583	0.040900	

Table 1. Cont.

Biomass	Samples	Synthesis Methods	Surface Area (m ² /g)	Total Pore (cm ³ /g)	Ref.
Eucalyptus globulus leaves	Ni-Fe/Escott-BEA/BC	Impregnation and pyrolysis	96	5.0	[61]
	Ni-Fe/BEA/BC		97	5.1	
	Ni-Fe/Escott		107	0.17	
	BC	Pyrolysis	74	4.8	
Woody pulp	f-WPB	Water and Microwave treatment followed by pyrolysis and HNO ₃	31.38	0.0381	[62]
	MoS ₂ -NFs		27.02	0.0727	
	MoS ₂ -NFs/f-WPB	One-pot hydrothermal method	15.95	0.0487	
Avocado seeds	Biochar	Pretreatment and pyrolysis	12	0.03	[63]
	5 wt% Ca loaded	Precipitation method	28	0.04	
	10 wt% Ca loaded		16	0.04	
	20 wt% Ca loaded		253	0.19	
α-cellulose	S ₁ -CF PC	Microwave	61.045	0.060	[64]
	S ₁ -CF C	Microwave	27.320	0.032	
	S ₁ -CF C ₅₀₀	Pyrolysis	42.420	0.053	

BC: Biochar Escott/Clinoptilolite zeolite.

Zhang et al. proposed that, in the synthesis of biochar-based composite Fe₃O₄/BC, the porosity was increased due to the reduction of organic content in biochar during the formation of iron oxide/biochar hybrid particles during the pyrolysis process. However, once excess nanoparticles are added to the biochar supports, the specific surface area may be reduced, such as BPC/nano zero-valent iron [59] and BC/MgO [57]. From the perspective of nanoscale particles, isolated CuO₂ exhibits a specific surface area of 15.7 m²/g. However, when loaded onto a biochar-based catalyst, the composite material's specific surface area can be significantly enhanced, reaching 30.3 m²/g [60]. Yan et al. proposed the incorporation of Clinoptilolite zeolite (Escott) into a Ni/Fe bimetallic catalyst supported on synthetic zeolite (BEA) [61]. The resulting composite material demonstrated enriched mesoporous surface area and mesoporous volume through catalytic hydrolysis, promoting the decomposition of biomass into gaseous and liquid products and increasing its porosity. Subsequently, pretreated biomass plays a non-negligible role in increasing the specific surface area. Biochar-based materials using rice husks as biomass are activated by KOH. The specific surface area of activated biochar is three times greater than that of inactivated biochar [59]. Biochar derived from Balsa wood powder is activated by the same pre-treatment; its specific surface area also showed a nearly two-fold increase [60]. As for the choice of pretreatment, the use of H₂SO₄ activation and the post-loading MnO₂ method were proposed. H₂SO₄ plays a dual role in pretreatment, helping to form holes on the biomass surface to increase the specific surface area and promoting the synergistic effect of -SO₃H by the introduction of MnO₂ [56].

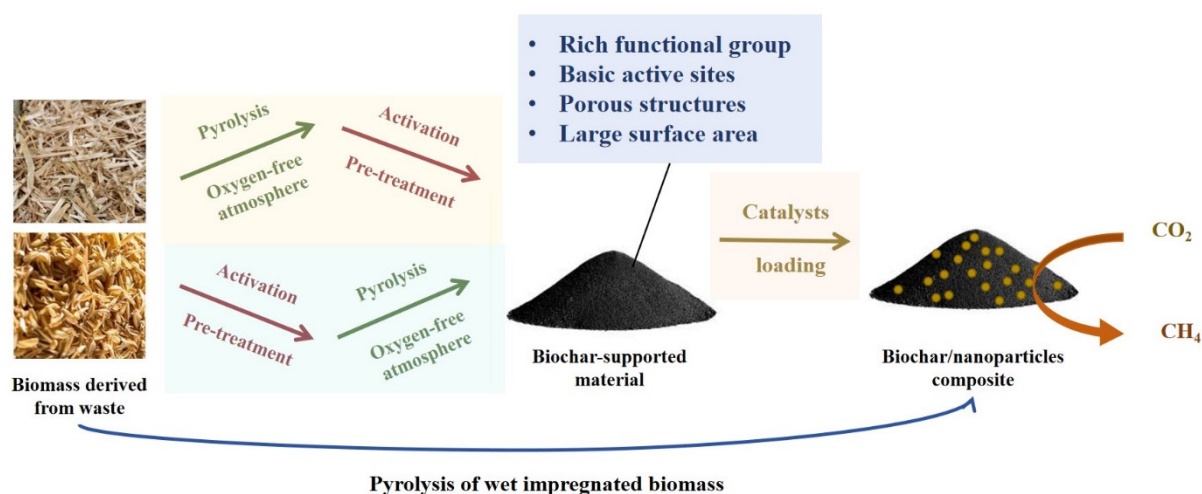
As a base material, biochar can have a surface area and total pore volume of 1503 m²/g when appropriate precursors and preferred pyrolysis parameters are selected [59], demonstrating that the raw material and preparation method play important roles in the final pore characteristics.

3. Case Studies for Catalyzed CO₂ Methanation

Research on biochar-based composite materials for catalyzing carbon dioxide methanation reveals the critical factors of temperature, pressure, and gas composition in CO₂ conversion rates and CH₄ selectivity. The preparation, pre-treatment/activation, nanoparticle modifications, and pyrolysis process parameters (temperature, flow rate, heat rate, residence time) play a key role in incorporating specific elements or achieving surface modifications (Scheme 2). In Table 2, we summarize the literature on some biochar-based composites for CO₂ methanation. The % CO₂ conversion and the % CH₄ selectivity were calculated according to Equations (3) and (4), where the subscripts “in” and “out” represent the participating gas inlet and gas outlet quantities, respectively.

$$\text{CO}_2 \text{ conversion} = \frac{\text{CO}_{2,\text{in}} - \text{CO}_{2,\text{out}}}{\text{CO}_{2,\text{in}}} \times 100 \quad (3)$$

$$\text{CO}_4 \text{ selectivity} = \frac{\text{CH}_{4,\text{out}}}{\text{CH}_{4,\text{out}} + \text{Other produced gases}_{,\text{out}}} \times 100 \quad (4)$$



Scheme 2. Flow chart of the synthesis of biochar-based catalysts for CO₂ methanation.

Table 2. Shortlisted biochar/catalyst composites and their application.

Biomass	Biochar/Catalyst (Yield%)	Synthesis Procedure	CO ₂ Methanation Performance	Refs.
Sucrose (Silica gel as a template)	Biochar/Ni-Fe	Biochar was prepared in two steps: pyrolysis at 600 °C in N ₂ followed by heat treatment again of the resulting biochar at 900 °C. NiFe bimetallic catalyst was prepared from mixture of nickel and iron nitrates. Biochar was wet-impregnated in NiFe solution. The mixture was carbonized at 300 °C for 8 h under H ₂ /N ₂ atmosphere for the biochar/NiFe.	CO ₂ conversion: 40% CH ₄ selectivity: 90% (400 °C under H ₂ :CO ₂ ratio of 4)	[65]

Table 2. Cont.

Biomass	Biochar/Catalyst (Yield%)	Synthesis Procedure	CO ₂ Methanation Performance	Refs.
Municipal solid waste (MSW, includes kitchen waste 25 wt%, paper 10 wt%, cloth and fiber 25 wt%, plastic 20 wt%, residue 20 wt%)	Biochar/Ni	A total of 100 g MSW was pyrolyzed at 600 °C in N ₂ (100 mL/min). A total of 20 g biochar was wet-impregnated into the 200 mL ethanol solution with 24.8 g nickel nitrate. Then, the mixture was calcined in N ₂ at 400 °C for 2 h and then calcined with H ₂ at 400 °C for 2 h for biochar/Ni.	CO ₂ conversion: ≥90% CH ₄ selectivity: ≥95% (1 MPa and 400 °C for 10 h)	[50]
Wheat straw pellets (9 mm OD and 10–13 mm long)	Biochar/Ni-CeO ₂	Biochar was produced via a two-step process: pyrolysis of biomass under N ₂ at 0.1 MPa and 500 °C (heating rate of 5 °C/min), and subsequent physical activation with CO ₂ at 1.0 MPa and 700 °C. CeO ₂ -doped biochar support (BBCe) was prepared via wet impregnation in Ce(NO ₃) ₃ ·6H ₂ O solution and calcination at 500 °C in an Ar atmosphere. Then, the nickel was deposited on BCCe supports via wet impregnation with Ni(NO ₃) ₂ ·6H ₂ O solution and calcined in air at 500 °C for biochar/NiCeO ₂ .	CO ₂ conversion: ≥60% CH ₄ selectivity: ≥90% (0.1 MPa and 375 °C for 10 h)	[66]
Commercial microcrystalline cellulose	Biochar/Pt Biochar/Pt-Na	Pyrolysis of biomass prepared at 500 °C for 2 h (heating rate 10 °C/min) in a reductant flow (1:1 nitrogen/hydrogen, 200 mL·min ⁻¹). Pt and Pt-Na-promoted catalysts were prepared by wetness impregnation. The aqueous solution of Pt(NH ₃) ₂ (NO ₂) ₂ alone or with Na ₂ CO ₃ was dropped on the biochar support, and the mixture was maintained under continuous stirring for 1 h (metal loading 1 wt% for platinum and 5 wt% for sodium). Then, the solid was dried and reduced at 350 °C for 1 h in N ₂ /H ₂ flow.	CO methanation reaction	[67]

Table 2. Cont.

Biomass	Biochar/Catalyst (Yield%)	Synthesis Procedure	CO ₂ Methanation Performance	Refs.
Pinus sylvestris	Biochar/Ni-Ce	Pinus sylvestris powder was added into a cerium nitrate solution until dried. The powder product was then ground uniformly with NaHCO ₃ . The mixture was heated up to 600 °C under N ₂ for 1 h. The black powder was impregnated with HNO ₃ (0.5 M) and then rinsed with deionized water until the filtered water was neutral. The resulting sample was then dried. The Ce-ABC was added in ethanol within Ni(NO ₃) ₂ ·6H ₂ O. The obtained solid sample was then dried and calcined at 500 °C for 4 h to give biochar/NiCe.	CO ₂ conversion: 88.6% CH ₄ selectivity: 92.3% (360 °C and 1 MPa)	[68]
Pinus sylvestris	Biochar/Ru-N	Biomass, urea, and NaHCO ₃ were mixed (with mass ratio of 1:4:3). The mixture was heated at 500–700 °C for 1 h under N ₂ atmosphere. The biochar was then impregnated with HNO ₃ and washed with deionized water and then dried to give N-doped biochar. A modified wet-impregnation method was used to prepare a Ru-based catalyst by adding N-doped biochar to ethanol containing RuCl ₃ ·xH ₂ O (Ru loading is 3 wt%). The mixture was oil-bath-treated and dried before being calcined at 480 °C for 4 h.	CO ₂ conversion: 93.8% CH ₄ selectivity: 99.7% (1 MPa and 460 °C, n(H ₂)/n(CO ₂) = 4)	[69]
Sugarcane bagasse	Biochar/Ni	Biomass impregnated into aqueous solution with nickel nitrate. The mixture underwent pyrolysis at 500 °C for 1 h under N ₂ atmosphere to obtain Ni-doped biochar.	CO ₂ conversion: 44% CH ₄ selectivity: 76% (1 Mpa and 400 °C)	[24]

3.1. The Role of Biochar Composite Preparation in CO₂ Methanation

The preparation of modified biochar composite materials typically involves a multi-step process, with variations in pre-treatment and pyrolysis steps, as illustrated in Table 2. González-Castaño et al. [65] introduced the infiltration of silica gel as a template into sucrose, followed by three rounds of impregnation and calcination to obtain a biochar support, as well as subsequent calcination and impregnation steps to produce Ni-Fe bimetallic catalysts. Renda et al. [66] emphasized biochar modification as a distinct step, involving pyrolysis under nitrogen and activation with CO₂, leading to impregnation of CeO₂ and the eventual preparation of nickel catalysts. Wang et al. [69] focused on the in situ pyrolysis process for nitrogen-doped biochar, utilizing *Pinus sylvestris* as biomass, urea as a nitrogen precursor, and NaHCO₃ for activation, followed by the loading of ruthenium catalysts.

For the pyrolysis steps, regardless of the single metal catalyst Ni/biochar composite [50], the biomass-soaked mixture was first calcined in N₂ at 400 °C for 2 h and then in H₂ at 400 °C for an additional period of 2 h. A bimetallic catalyst NiFe/biochar composite [65] was obtained by a second pyrolysis of the biochar-soaked mixture, conducted at 300 °C for

8 h under a N₂/H₂ gas mixture stream. It was observed that the temperature set during the second pyrolysis did not exceed that used in the initial pyrolysis step.

3.2. Effect of Surface Basic Sites

Considering that CO₂ is weakly acidic, the basic groups on the surface of carbonaceous materials play a significant role in the adsorption/activation of CO₂. Santos et al. [67] prepared Na/Pt-biochar composites using alkali metals, as the latter can change the electronic structure of the Pt-biochar, thus improving CO₂ adsorption on the Pt catalyst and creating additional new basic sites for CO₂ activation.

In a related study, Mei et al. [50] highlighted the importance of acid-soluble inorganics and water-soluble inorganics over the biochar-supported Ni catalyst for methanation reaction at 1 MPa and 400 °C for 10 h. The authors emphasized the role of alkaline inorganic material on the biochar surface. Surface modification was performed through pretreatment to inhibit acid-soluble inorganics and water-soluble inorganics on biochar. The results showed that nickel-loaded biochar without pretreatment resulted in higher CO₂ conversion, indicating that acid-soluble inorganics dominate the performance of biochar, while water-soluble inorganics also play a role, but to a lesser extent. Acid-soluble inorganics can not only promote the interaction of Ni/support but also increase the concentration of basic sites on the catalyst surface.

Wang et al. [69] investigated the role of the three types of nitrogen on the surface alkalinity of biochar composites. They achieved a CO₂ conversion of 93.8% and a CH₄ selectivity of 99.7% using high-performance Ru/N-ABC-600. It was emphasized that the high pyridinic nitrogen content and the surface basicity of the catalyst are the key factors for superior performance, as depicted in Figure 5. Indeed, the CO₂ conversion levels off at 380 °C, with a clear correlation with the extent of the pyridinic nitrogen in the biochar support, as determined by N1s peak-fitting in XPS. The incorporation of nitrogen atoms, especially pyridinic-N, enhance the electronic effects and alkalinity, promoting H₂ dissociation and CO₂ adsorption. Metal doping represents an indispensable methodology, enhancing the performance and stability of Ni-based catalysts supported on the biochar.

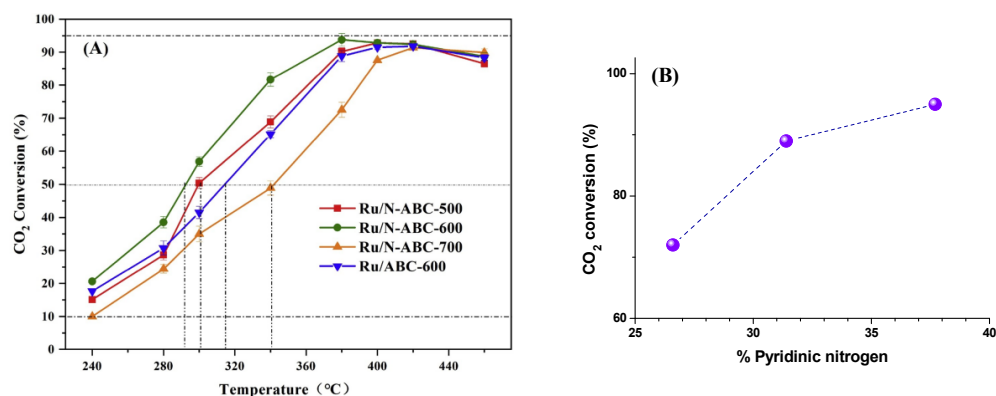


Figure 5. CO₂ conversion of ruthenium-loaded nitrogen-doped biochar prepared at 500–700 °C (A), and plot of CO₂ conversion (in%) to the percentage of biochar pyridinic nitrogen (B). Figure 5A is reproduced from ref. [70] with permission of Elsevier.

González-Castagno et al. [65] used the CO₂-thermal programmed desorption (TPD) to determine the surface basic sites as well as the reaction rates and turnover frequencies (TOFs), which are calculated as follows:

$$\text{TOF (s}^{-1}\text{)} = \frac{\text{mol}_{\text{CO}_2, \text{converted}}}{\text{S} \cdot \text{mol}_{\text{Ni}} \cdot \text{Dispersion}} \times 100$$

The authors determined the TOFs by considering the Ni sites dispersed on the surface of the catalysts and compared in this way Ni/Al vs. NiFe/Al and Ni/biochar vs.

NiFe/biochar. They found that surface basicity contributes to the activation and adsorption of CO₂, which is favored by the increase in basic sites (Table 3). Therefore, the extent of basic sites was correlated with catalytic performance, but within the set of samples having the same support. If one compares the catalysts loaded on different supports, the basic site density promotes CO₂ adsorption but not necessarily the TOF. Indeed, NiFe/biochar adsorbs less CO₂ than NiFe/Al but performs much better than the latter when one considers TOF; this is ascribed to the remarkable specific surface area imparted by the underlying biochar (712 >> 162 m²/g).

Table 3. Surface area, Ni particle dispersion, basic sites, CO₂ adsorption, and TOFs for biochar-catalyst composites.

	Surface Area (m ² g ⁻¹)	Ni Particle Dispersion (%)	Ni Particle Size (nm)	Basic Site Density (μmol m ⁻²)	CO ₂ Adsorption (μmol g _{cat} ⁻¹)	TOF (10 ³ s ⁻¹)
Ni/Al	168	13	8	1.89	308.5	0.81
NiFe/Al	162	18	6	2.26	379.1	1.52
Ni/biochar	754	9	13	–	120.9	0.63
NiFe/biochar	712	10	11	0.2	140.8	3.12

Following the successful bimetallic Ni/Ce-biochar composite synthesis, Di Stasi et al. [70] considered replacing the Ce catalyst with an N-catalyst (using urea) over the Ni-biochar support. The addition of nitrogen imparted higher catalytic activity due to the higher pyridinic-N content introduced by urea doping, and nitrogen-containing functional group content remained relatively constant under the operational conditions. However, the N-catalyst did not significantly improve the dispersion of Ni nanoparticles as CeNi did.

3.3. Effect of Nanometal Dispersion

Ni/ABC retains most of the specific surface area of the pristine biochar (more than 350 m²/g); the specific surface area of the catalyst Ni/CeO₂ is only 6.4 m²/g. After in situ modification of cerium, the specific surface area of the Ni/Ce-ABC is almost half that of Ni/ABC, at about 155.6 m²/g. However, the modification of Ce also helps to improve the nanoparticle dispersion on the biochar and limits the growth of nickel species, reducing the average size of Ni from 20 nm for Ni/ABC to 5–12 nm in the case of Ni/Ce-ABC. Of utmost importance, Ni nanoparticles are evenly distributed on the support. The Ni/Ce-ABC composite shows better performance at a relatively lower temperature (300 °C), which can be mainly attributed to the uniform dispersion of nickel species and CeO₂ particles, providing more alkaline sites for CO₂ adsorption and activation. When the temperature increases to 360 °C, the CO₂ conversion% of the three catalysts is almost the same, which may be due to the similar Ni content in all composites (Figure 6). The reaction activity of the catalyst under high temperature mainly depends on Ni species.

3.4. Effect of Metal Loading

Renda et al. [66] further studied the effect of CeO₂ doping amount on Ni-biochar (obtained from wheat straw) on CO₂ methanation and stability. Figure 7 shows that the addition of CeO₂ enhances catalytic performance by promoting CO₂ activation and reduces the deactivation rate of Ni-biochar support for CH₄ yield, indicating that CeO₂ strengthens Ni-support interaction to increase catalyst life. The specific surface area of BC may be tuned using CeO₂; adding a low concentration (10 wt%) of metal nanoparticles resulted in a higher specific surface area and micropore volume. In contrast, when exceeding a certain amount (50 wt%), the metal nanoparticles completely coat the biochar and block its pores, therefore resulting in a very low specific surface area and, consequently, a lower CO₂ conversion rate.

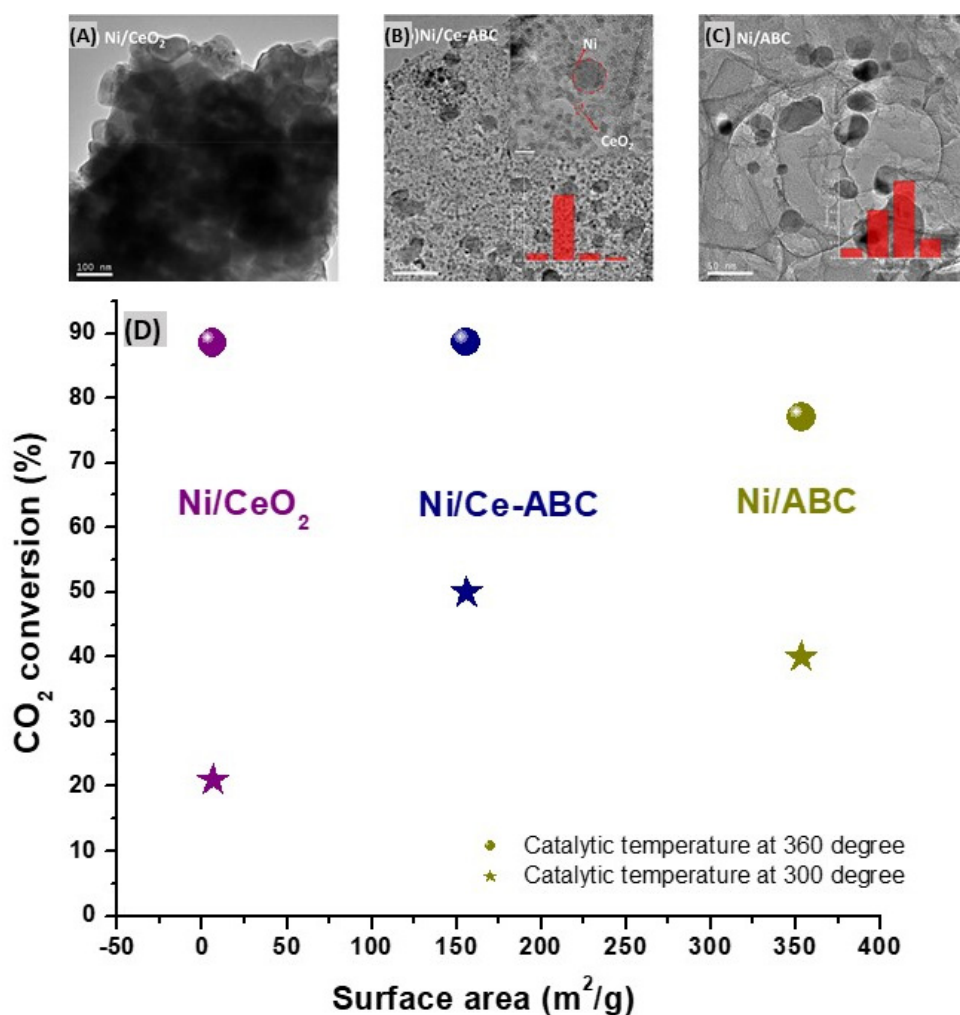


Figure 6. TEM images of Ni/CeO₂ (A), Ni/Ce-ABC (B), and Ni/ABC (C) and plot of CO₂ conversion to surface area of catalyst (D). (A–C) are reproduced from [68] with permission of Elsevier.

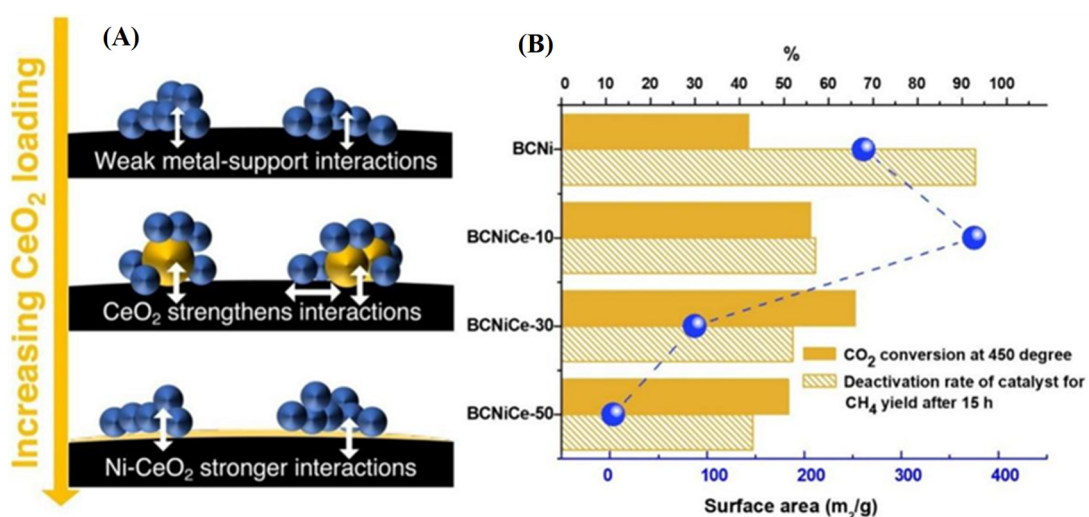


Figure 7. Model diagram of CeO₂ doping amount on Ni-biochar (A); CO₂ conversion, deactivation rate, and surface area of catalyst (B). (A) is reproduced from [66] with permission of Elsevier.

In another study [70], the same research group compared different concentrations of Ce and Ni on the wheat straw biochar substrate and revealed that a biochar-based composite with 30% Ce and 20% Ni exhibited optimal carbon dioxide conversion (>90%) and methane selectivity (~100%) at 350 °C and 1.0 MPa.

Gamal et al. [24] developed an interesting eco-friendly sugarcane bagasse biochar/nickel sustainable catalyst (Figure 8a) for the thermal catalytic CO₂ methanation (Figure 8b). The biochar-supported Ni catalyst prepared by pyrolysis of 0.5 mmol Ni-impregnated gram of biomass exhibited the highest CO₂ conversion efficiency (Figure 8c,d) when tested in the 250–550 °C temperature range. This was ascribed to the good dispersion of ~3 nm sized Ni particles on the biochar surface, in sufficient concentration. Further studies have revealed that highest CH₄ selectivity (Figure 8c) is observed at 400 °C and 1 bar pressure (44% CO₂ conversion; 76% methane selectivity; 34% methane yield). The authors found the TOF to be highest for biochar made from 0.5 mmol nickel salt per gram of SCB. The 0.5Ni/SCBB catalyst enabled the transformation of a large number of molecules within a short period of reaction time, regardless the operating working temperature (Figure 8d). Moreover, the Ni/biochar optimized catalyst was found to be highly stable and could be re-used for the same process. The green and low-cost strategy devised by the authors could be extended to other reductive catalysts.

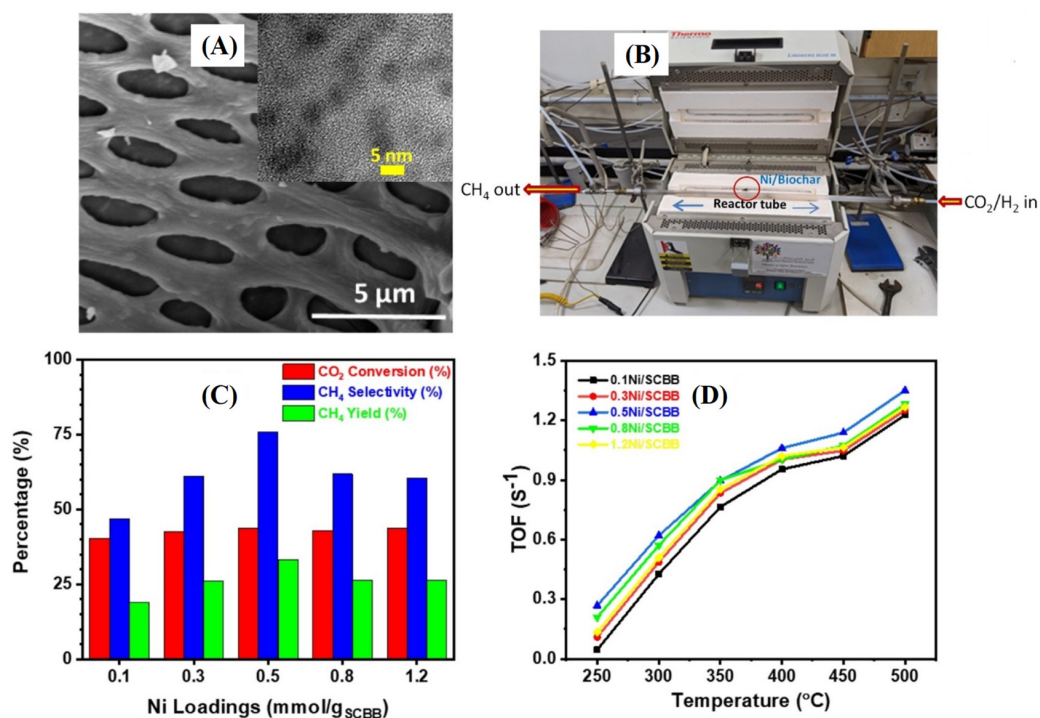


Figure 8. Properties and performance of Ni/SCBB composite catalysts: (A) SEM picture of 0.5Ni/SCBB; TEM is shown in inset; (B) CO₂ methanation experimental setup; (C) CO₂ conversion; CH₄ selectivity and yield; (D) TOF for Ni/SCBB composites. Reproduced from ref. [24] with permission of Elsevier.

4. Challenges and Prospects of Biochar catalyst Composites in CO₂ Methanation

In recent years, biochar-based composites have been rapidly developed for CO₂ capture [71–73]. The structural characteristics and surface functional groups of biochar supports are crucial for the effective reduction of CO₂ to CH₄, and the fabrication and modification of biochar catalyst composite materials are also critical. As mentioned earlier, metal-loaded catalysts exhibit broad practical prospects due to their simple preparation methods, superior catalytic performance, and good stability. Among them, nickel-based catalysts are extensively applied and researched owing to their outstanding CO₂ methanation performance and facilitate recovery, thus holding significant potential for energy

utilization. However, metal nanoparticles tend to aggregate on the surface of biochar, and the CO₂ methanation process requires relatively high temperatures and high pressures. Highly porous biochar is an excellent support for nickel, but the addition of another oxide as an intermediate support of nickel for dry gas reforming [74], which results in ternary biochar-oxide- Ni system, seems to be recommended for excellent dispersion of nickel and high catalytic efficiency, at even lower temperature [68]. Thus, in order to better satisfy industrial application requirements, researchers need to conduct further studies and developments to improve the performance of composite catalysts, enabling large-scale green energy utilization under mild reaction conditions. Furthermore, encouraging the production of carbon-containing materials from agricultural waste is a promising approach, which contributes to the creation of environmentally friendly and nearly cost-free support materials while reducing the adverse environmental impact of agricultural waste. Therefore, biochar-based composite materials show potential and prospects as catalysts for environmental remediation in the future.

5. Conclusions

In this review, we first presented the fabrication and modification of biochar-immobilized nanoparticle catalyst composites and focused on the conversion of biomass into valuable products with thermochemical methods. The activation processes and metal nanoparticle loading are key steps for the modification of biochar catalyst composite materials, suggesting the need to improve the physicochemical properties, such as graphitization, surface functional groups, and active sites. Notably, the pore structure of biochar-supported composites is impacted by the sequence of wet impregnation and pyrolysis. Secondly, in the application of CO₂ methanation with biochar catalyst composites, the alkaline sites on the material surface are closely linked to CO₂ adsorption. However, whenever the extent of basic sites decreases, a high specific area is required to counterbalance the loss of basic sites. In this respect, biochar is shown to provide an excellent alternative to traditional supports such as alumina. Concerning metal loading onto the biochar, although it might induce a decrease in the surface area, there is an increase in micropore volume, thus facilitating easier gas molecule diffusion. The introduction of metal nanoparticles also contributes to an increase in the active sites, and bimetallic catalyst nanoparticles effectively mitigate the aggregation of nanoparticles, achieving higher dispersion on the composite material surface and thereby enhancing CO₂ conversion rates and CH₄ selectivity.

These research findings offer reliable insights into the preparation and modification of biochar catalyst composite materials, facilitating further optimization of such products to CO₂ methanation applications.

Author Contributions: Conceptualization (M.M.C., M.T., A.G. and A.M.A.); methodology (M.M.C., M.T. and A.G.); validation (M.T., A.G., A.K.B., K.J., A.M.A. and M.M.C.); writing—original draft (M.T., A.G., A.K.B. and M.M.C.); writing—review and editing (M.T., A.G., A.K.B., K.J., A.M.A. and M.M.C.); supervision (M.M.C.); funding acquisition (M.M.C., A.K.B., M.T. and A.M.A.). All authors have read and agreed to the published version of the manuscript.

Funding: This work was supported by (i) the China Scholarship Council for the provision of PhD scholarship to M. Tang (No 202008310221); (ii) the Qatar National Research Fund (QNRF, a member of the Qatar Foundation) through the National Priority Research Program Grant (NPRP) NPRP13S-0117-200095; (iii) Qatar University through an International Research Collaboration Co-Fund grant, IRCC-2021-015; and (iv) Wallonie Bruxelles International (WBI) for the provision of a grant to A.K. Bhakta through “Bourse WBI Excellence World” (No. Imputation 101386, Article Budgétaire 13 33.01.00.07).

Data Availability Statement: The data presented in this study are available on request from the corresponding author.

Conflicts of Interest: The authors declare no conflict of interest.

References

1. Jones, M.W.; Peters, G.P.; Gasser, T.; Andrew, R.M.; Schwingshackl, C.; Guetschow, J.; Houghton, R.A.; Friedlingstein, P.; Pongratz, J.; Le Quere, C. National contributions to climate change due to historical emissions of carbon dioxide, methane, and nitrous oxide since 1850. *Scientific Data* **2023**, *10*, 155. [[CrossRef](#)]
2. Zhu, D.D.; Liu, J.L.; Qiao, S.Z. Recent Advances in Inorganic Heterogeneous Electrocatalysts for Reduction of Carbon Dioxide. *Adv. Mater.* **2016**, *28*, 3423–3452. [[CrossRef](#)] [[PubMed](#)]
3. Jacobson, T.A.; Kler, J.S.; Hernke, M.T.; Braun, R.K.; Meyer, K.C.; Funk, W.E. Direct human health risks of increased atmospheric carbon dioxide. *Nat. Sustain.* **2019**, *2*, 691–701. [[CrossRef](#)]
4. Mac Dowell, N.; Fennell, P.S.; Shah, N.; Maitland, G.C. The role of CO₂ capture and utilization in mitigating climate change. *Nat. Clim. Chang.* **2017**, *7*, 243–249. [[CrossRef](#)]
5. Dziejarski, B.; Serafin, J.; Andersson, K.; Krzyzyska, R. CO₂ capture materials: A review of current trends and future challenges. *Mater. Today Sustain.* **2023**, *24*, 100483. [[CrossRef](#)]
6. Chaemchuen, S.; Semyonov, O.V.; Dingemans, J.; Xu, W.; Zhuiykov, S.; Khan, A.; Verpoort, F. Progress on catalyst development for direct synthesis of dimethyl carbonate from CO₂ and methanol. *Chem. Afr.* **2019**, *2*, 533–549. [[CrossRef](#)]
7. Zhang, M.; Gao, Y.; Mao, Y.; Wang, W.; Sun, J.; Song, Z.; Sun, J.; Zhao, X. Enhanced dry reforming of methane by microwave-mediated confined catalysis over Ni-La/AC catalyst. *Chem. Eng. J.* **2023**, *451*, 138616. [[CrossRef](#)]
8. Gamal, A.; Eid, K.; Abdullah, A.M. Engineering of Pt-based nanostructures for efficient dry (CO₂) reforming: Strategy and mechanism for rich-hydrogen production. *Int. J. Hydrogen Energy* **2022**, *47*, 5901–5928. [[CrossRef](#)]
9. Yan, P.H.; Peng, H.; Vogrin, J.; Rabiee, H.; Zhu, Z.H. Selective CO₂ hydrogenation over zeolite-based catalysts for targeted high-value products. *J. Mater. Chem. A* **2023**, *11*, 17938–17960. [[CrossRef](#)]
10. Xie, Y.; Wen, J.; Li, Z.; Chen, J.; Zhang, Q.; Ning, P.; Hao, J. Double-Edged Sword Effect of Classical Strong Metal–Support Interaction in Catalysts for CO₂ Hydrogenation to CO, Methane, and Methanol. *ACS Mater. Lett.* **2023**, *5*, 2629–2647. [[CrossRef](#)]
11. Malik, M.I.; Achouri, I.E.; Abatzoglou, N.; Gitzhofer, F. Intensified performance of methane dry reforming based on non-thermal plasma technology: Recent progress and key challenges. *Fuel Process. Technol.* **2023**, *245*, 107748. [[CrossRef](#)]
12. Ali, S.; Khader, M.M.; Almarri, M.J.; Abdelmoneim, A.G. Ni-based nano-catalysts for the dry reforming of methane. *Catal. Today* **2020**, *343*, 26–37. [[CrossRef](#)]
13. Khader, M.M.; Al-Marri, M.J.; Ali, S.; Abdelmoneim, A.G.; Kumar, A.; Saleh, M.A.H.; Soliman, A. Catalytic evaluation of Ni-based nano-catalysts in dry reformation of methane. In Proceedings of the 2017 IEEE 17th International Conference on Nanotechnology (IEEE-NANO), Pittsburgh, PA, USA, 25–28 July 2017; pp. 1051–1055.
14. Song, L.; Wang, H.; Wang, S.; Qu, Z. Dual-site activation of H₂ over Cu/ZnAl₂O₄ boosting CO₂ hydrogenation to methanol. *Appl. Catal. B Environ.* **2023**, *322*, 122137. [[CrossRef](#)]
15. Hussain, I.; Jalil, A.A.; Izan, S.M.; Azami, M.S.; Kidam, K.; Airirazali, N.; Ripin, A. Thermodynamic and experimental explorations of CO₂ methanation over highly active metal-free fibrous silica-beta zeolite (FS@SiO₂-BEA) of innovative morphology. *Chem. Eng. Sci.* **2021**, *229*, 116015. [[CrossRef](#)]
16. Guo, X.; Traitangwong, A.; Hu, M.; Zuo, C.; Meeyoo, V.; Peng, Z.; Li, C. Carbon Dioxide Methanation over Nickel-Based Catalysts Supported on Various Mesoporous Material. *Energy Fuels* **2018**, *32*, 3681–3689. [[CrossRef](#)]
17. Mateus, F.; Teixeira, P.; Lopes, J.M.; Henriques, C.; Bacariza, C. CO₂ Methanation on Ni Catalysts Supported over Activated Carbons Derived from Cork Waste. *Energy Fuels* **2023**, *37*, 8552–8562. [[CrossRef](#)]
18. Omiri, J.; Snoussi, Y.; Bhakta, A.K.; Truong, S.; Ammar, S.; Khalil, A.M.; Jouini, M.; Chehimi, M.M. Citric-Acid-Assisted Preparation of Biochar Loaded with Copper/Nickel Bimetallic Nanoparticles for Dye Degradation. *Colloids Interfaces* **2022**, *6*, 18. [[CrossRef](#)]
19. Boubkr, L.; Bhakta, A.K.; Snoussi, Y.; Da Silva, C.M.; Michely, L.; Jouini, M.; Ammar, S.; Chehimi, M.M. Highly Active Ag-Cu Nanocrystal Catalyst-Coated Brewer’s Spent Grain Biochar for the Mineralization of Methyl Orange and Methylene Blue Dye Mixture. *Catalysts* **2022**, *12*, 1475. [[CrossRef](#)]
20. Bayoka, H.; Snoussi, Y.; Bhakta, A.K.; El Garah, M.; Khalil, A.M.; Jouini, M.; Ammar, S.; Chehimi, M.M. Evidencing the synergistic effects of carbonization temperature, surface composition and structural properties on the catalytic activity of biochar/ bimetallic composite. *J. Anal. Appl. Pyrolysis* **2023**, *173*, 106069. [[CrossRef](#)]
21. Tang, M.; Snoussi, Y.; Bhakta, A.K.; El Garah, M.; Khalil, A.M.; Ammar, S.; Chehimi, M.M. Unusual, hierarchically structured composite of sugarcane pulp bagasse biochar loaded with Cu/Ni bimetallic nanoparticles for dye removal. *Environ. Res.* **2023**, *232*, 116232. [[CrossRef](#)]
22. Tripathi, M.; Sahu, J.N.; Ganesan, P. Effect of process parameters on production of biochar from biomass waste through pyrolysis: A review. *Renew. Sustain. Energy Rev.* **2016**, *55*, 467–481. [[CrossRef](#)]
23. Geça, M.; Khalil, A.M.; Tang, M.; Bhakta, A.K.; Snoussi, Y.; Nowicki, P.; Wiśniewska, M.; Chehimi, M.M. Surface Treatment of Biochar—Methods, Surface Analysis and Potential Applications: A Comprehensive Review. *Surfaces* **2023**, *6*, 179–213. [[CrossRef](#)]
24. Gamal, A.; Tang, M.; Bhakta, A.K.; Snoussi, Y.; Khalil, A.M.; Jlassi, K.; Chehimi, M.M.; Ali, A.M.A. CO₂ methanation using sugarcane bagasse biochar/nickel sustainable catalysts. *Mater. Today Sustain.* **2024**, *25*, 100627. [[CrossRef](#)]
25. Zhang, S.-Z.; Cui, Z.-S.; Zhang, M.; Zhang, Z.-H. Biochar based functional materials as heterogeneous catalysts for organic reactions. *Curr. Opin. Green Sustain. Chem.* **2022**, *38*, 100713. [[CrossRef](#)]

26. Velusamy, K.; Devanand, J.; Kumar, P.S.; Soundarajan, K.; Sivasubramanian, V.; Sindhu, J.; Vo, D.-V.N. A review on nano-catalysts and biochar-based catalysts for biofuel production. *Fuel* **2021**, *306*, 121632. [[CrossRef](#)]
27. Ramos, R.; Abdelkader-Fernández, V.K.; Matos, R.; Peixoto, A.F.; Fernandes, D.M. Metal-supported biochar catalysts for sustainable biorefinery, electrocatalysis, and energy storage applications: A review. *Catalysts* **2022**, *12*, 207. [[CrossRef](#)]
28. Dihingia, H.; Tiwari, D. Impact and implications of nanocatalyst in the Fenton-like processes for remediation of aquatic environment contaminated with micro-pollutants: A critical review. *J. Water Process Eng.* **2022**, *45*, 102500. [[CrossRef](#)]
29. Zhu, X.; Labianca, C.; He, M.; Luo, Z.; Wu, C.; You, S.; Tsang, D.C. Life-cycle assessment of pyrolysis processes for sustainable production of biochar from agro-residues. *Bioresour. Technol.* **2022**, *360*, 127601. [[CrossRef](#)]
30. Yaashikaa, P.; Kumar, P.S.; Varjani, S.J.; Saravanan, A. Advances in production and application of biochar from lignocellulosic feedstocks for remediation of environmental pollutants. *Bioresour. Technol.* **2019**, *292*, 122030. [[CrossRef](#)]
31. Wan, J.; Liu, L.; Wang, G.; Sang, L.; Liang, W.; Zhang, W.; Peng, C.; Fu, R. Unveiling the mechanisms of carbon conversion and loss in biochars derived from characteristic lignocellulosic biomass. *J. Environ. Chem. Eng.* **2022**, *10*, 108403. [[CrossRef](#)]
32. Bhakta, A.K.; Tang, M.; Snoussi, Y.; Khalil, A.M.; Mascarenhas, R.J.; Mekhalif, Z.; Abderrabba, M.; Ammar, S.; Chehimi, M.M. Sweet, salty, sour, and romantic biochar-supported ZnO: Highly active composite catalysts for environmental remediation. *Emergent Mater.* **2023**, 1–15. [[CrossRef](#)]
33. Zanchetta, E.; Damergi, E.; Patel, B.; Borgmeyer, T.; Pick, H.; Pulgarin, A.; Ludwig, C. Algal cellulose, production and potential use in plastics: Challenges and opportunities. *Algal Res.* **2021**, *56*, 102288. [[CrossRef](#)]
34. Sharma, A.K.; Ghodke, P.K.; Goyal, N.; Bobde, P.; Kwon, E.E.; Lin, K.Y.; Chen, W.H. A critical review on biochar production from pine wastes, upgradation techniques, environmental sustainability, and challenges. *Bioresour. Technol.* **2023**, *387*, 129632. [[CrossRef](#)] [[PubMed](#)]
35. Wen, C.; Liu, T.; Wang, D.; Wang, Y.; Chen, H.; Luo, G.; Zhou, Z.; Li, C.; Xu, M. Biochar as the effective adsorbent to combustion gaseous pollutants: Preparation, activation, functionalization and the adsorption mechanisms. *Prog. Energy Combust. Sci.* **2023**, *99*, 101098. [[CrossRef](#)]
36. Mishra, R.K.; Kumar, D.J.P.; Narula, A.; Chistie, S.M.; Naik, S.U. Production and beneficial impact of biochar for environmental application: A review on types of feedstocks, chemical compositions, operating parameters, techno-economic study, and life cycle assessment. *Fuel* **2023**, *343*, 127968. [[CrossRef](#)]
37. Ahuja, R.; Kalia, A.; Sikka, R.; Chaitra, P. Nano Modifications of Biochar to Enhance Heavy Metal Adsorption from Wastewaters: A Review. *ACS Omega* **2022**, *7*, 45825–45836. [[CrossRef](#)]
38. Xia, C.; Pathy, A.; Paramasivan, B.; Ganeshan, P.; Dhamodharan, K.; Juneja, A.; Kumar, D.; Brindhadevi, K.; Kim, S.-H.; Rajendran, K. Comparative study of pyrolysis and hydrothermal liquefaction of microalgal species: Analysis of product yields with reaction temperature. *Fuel* **2022**, *311*, 121932. [[CrossRef](#)]
39. Yu, S.; Wang, L.; Li, Q.; Zhang, Y.; Zhou, H. Sustainable carbon materials from the pyrolysis of lignocellulosic biomass. *Mater. Today Sustain.* **2022**, *19*, 100209. [[CrossRef](#)]
40. Sun, C.; Chen, T.; Huang, Q.; Zhan, M.; Li, X.; Yan, J. Activation of persulfate by CO₂-activated biochar for improved phenolic pollutant degradation: Performance and mechanism. *Chem. Eng. J.* **2020**, *380*, 122519. [[CrossRef](#)]
41. Iberahim, N.; Sethupathi, S.; Bashir, M.J.K.; Kanthasamy, R.; Ahmad, T. Evaluation of oil palm fiber biochar and activated biochar for sulphur dioxide adsorption. *Sci. Total Environ.* **2022**, *805*, 150421. [[CrossRef](#)]
42. Feng, D.; Guo, D.; Zhang, Y.; Sun, S.; Zhao, Y.; Chang, G.; Guo, Q.; Qin, Y. Adsorption-enrichment characterization of CO₂ and dynamic retention of free NH₃ in functionalized biochar with H₂O/NH₃•H₂O activation for promotion of new ammonia-based carbon capture. *Chem. Eng. J.* **2021**, *409*, 128193. [[CrossRef](#)]
43. Peter, A.; Chabot, B.; Loranger, E. Pre-and post-pyrolysis effects on iron impregnation of ultrasound pre-treated softwood biochar for potential catalysis applications. *SN Appl. Sci.* **2021**, *3*, 643. [[CrossRef](#)]
44. Tang, Z.; Gao, J.; Zhang, Y.; Du, Q.; Feng, D.; Dong, H.; Peng, Y.; Zhang, T.; Xie, M. Ultra-microporous biochar-based carbon adsorbents by a facile chemical activation strategy for high-performance CO₂ adsorption. *Fuel Process. Technol.* **2023**, *241*, 107613. [[CrossRef](#)]
45. Jabar, J.M.; Odusote, Y.A.; Ayinde, Y.T.; Yilmaz, M. African almond (*Terminalia catappa* L.) leaves biochar prepared through pyrolysis using H₃PO₄ as chemical activator for sequestration of methylene blue dye. *Results Eng.* **2022**, *14*, 100385. [[CrossRef](#)]
46. Nguyen, T.-B.; Truong, Q.-M.; Chen, C.-W.; Doong, R.-A.; Chen, W.-H.; Dong, C.-D. Mesoporous and adsorption behavior of algal biochar prepared via sequential hydrothermal carbonization and ZnCl₂ activation. *Bioresour. Technol.* **2022**, *346*, 126351. [[CrossRef](#)]
47. Snoussi, Y.; Sifaoui, I.; El Garah, M.; Khalil, A.M.; Jouini, M.; Ammar, S.; Morales, J.L.; Chehimi, M.M. Green, zero-waste pathway to fabricate supported nanocatalysts and anti-kinetoplastid agents from sugarcane bagasse. *Waste Manag.* **2023**, *155*, 179–191. [[CrossRef](#)] [[PubMed](#)]
48. Prabakaran, E.; Pillay, K.; Brink, H. Hydrothermal synthesis of magnetic-biochar nanocomposite derived from avocado peel and its performance as an adsorbent for the removal of methylene blue from wastewater. *Mater. Today Sustain.* **2022**, *18*, 100123. [[CrossRef](#)]
49. He, Z.; Zhang, Y.; Lv, J.; Zhou, S.; Niu, J.; Li, Z.; Wang, X.; Wagberg, T.; Hu, G. Microwave-assisted synthesis of amorphous cobalt nanoparticle decorated N-doped biochar for highly efficient degradation of sulfamethazine via peroxymonosulfate activation. *J. Water Process Eng.* **2022**, *50*, 103226. [[CrossRef](#)]

50. Mei, Z.; Chen, D.; Yuan, G.; Zhang, R. Waste-derived chars as methanation catalyst support: Role of inorganics in the char and its guide to catalyst design. *Fuel* **2023**, *349*, 128574. [[CrossRef](#)]
51. Marcinczyk, M.; Krasucka, P.; Bogusz, A.; Tomczyk, B.; Duan, W.; Pan, B.; Oleszczuk, P. Ecotoxicological characteristics and properties of zinc-modified biochar produced by different methods. *Chemosphere* **2023**, *315*, 137690. [[CrossRef](#)]
52. Leng, L.; Xiong, Q.; Yang, L.; Li, H.; Zhou, Y.; Zhang, W.; Jiang, S.; Li, H.; Huang, H. An overview on engineering the surface area and porosity of biochar. *Sci. Total Environ.* **2021**, *763*, 144204. [[CrossRef](#)]
53. Bagreev, A.; Bandosz, T.J.; Locke, D.C. Pore structure and surface chemistry of adsorbents obtained by pyrolysis of sewage sludge-derived fertilizer. *Carbon* **2001**, *39*, 1971–1979. [[CrossRef](#)]
54. Zhang, N.; Reguyal, F.; Praneeth, S.; Sarmah, A.K. A green approach of biochar-supported magnetic nanocomposites from white tea waste: Production, characterization and plausible synthesis mechanisms. *Sci. Total Environ.* **2023**, *886*, 163923. [[CrossRef](#)] [[PubMed](#)]
55. Kuang, Q.; Liu, K.; Wang, Q.; Chang, Q. Three-dimensional hierarchical pore biochar prepared from soybean protein and its excellent Cr (VI) adsorption. *Sep. Purif. Technol.* **2023**, *304*, 122295. [[CrossRef](#)]
56. Zhang, L.; Zhang, T.; Cai, Y.; Zhao, Y.; Song, S.; Quintana, M. Engineering sulfuric acid-pretreated biochar supporting MnO₂ for efficient toxic organic pollutants removal from aqueous solution in a wide pH range. *J. Clean. Prod.* **2023**, *416*, 137968. [[CrossRef](#)]
57. Shang, H.; Hu, W.; Li, Y.; Zhang, Q.; Feng, Y.; Xu, Y.; Yu, Y. Biochar-supported magnesium oxide as high-efficient lead adsorbent with economical use of magnesium precursor. *Environ. Res.* **2023**, *229*, 115863. [[CrossRef](#)]
58. Anthonysamy, S.I.; Ahmad, M.A.; Yahaya, N.K.E. Insight the mechanism of MgAl/layered double hydroxide supported on rubber seed shell biochar for Remazol Brilliant Violet 5R removal. *Arab. J. Chem.* **2023**, *16*, 104643. [[CrossRef](#)]
59. Li, X.; Wang, C.; Chen, X.; Li, D.; Jin, Q. Enhanced oxidation and removal of As (III) from water using biomass-derived porous carbon-supported nZVI with high iron utilization and fast adsorption. *J. Environ. Chem. Eng.* **2023**, *11*, 109038. [[CrossRef](#)]
60. Li, X.; Chen, J.; Wang, Y.; Cheng, Z.; Chen, X.; Gao, X.; Guo, M. Porous spherical Cu₂O supported by wood-based biochar skeleton for the adsorption-photocatalytic degradation of methyl orange. *Appl. Surf. Sci.* **2023**, *611*, 155744.
61. Yan, P.; Azreena, I.N.; Peng, H.; Rabiee, H.; Ahmed, M.; Weng, Y.; Zhu, Z.; Kennedy, E.M.; Stockenhuber, M. Catalytic hydrolysis of biomass using natural zeolite-based catalysts. *Chem. Eng. J.* **2023**, *476*, 146630. [[CrossRef](#)]
62. El-Sabban, H.A.; Attia, S.Y.; Mostafa, H.Y.; Mohamed, S.G. Rational design of MoS₂ nanoflowers grafted highly porous functionalized woody pulp-derived biochar for sustainable energy storage devices. *Fuel* **2024**, *359*, 130485. [[CrossRef](#)]
63. di Bitonto, L.; Reynel-Ávila, H.E.; Mendoza-Castillo, D.I.; Bonilla-Petriciolet, A.; Durán-Valle, C.J.; Pastore, C. Synthesis and characterization of nanostructured calcium oxides supported onto biochar and their application as catalysts for biodiesel production. *Renew. Energy* **2020**, *160*, 52–66. [[CrossRef](#)]
64. Zhou, Q.; Qin, L.; Yin, Z.; Jiang, H. Facile microwave assisted one-pot solid-state construction of Co-Fe spinel oxide/porous biochar for highly efficient 4-nitrophenol degradation: Effect of chemical blowing and surface vulcanization. *Sep. Purif. Technol.* **2024**, *328*, 125033. [[CrossRef](#)]
65. Gonzalez-Castano, M.; Morales, C.; Navarro de Miguel, J.C.; Boelte, J.H.; Klepel, O.; Flege, J.I.; Arellano-Garcia, H. Are Ni/ and Ni₅Fe₁/biochar catalysts suitable for synthetic natural gas production? A comparison with g-Al₂O₃ supported catalysts. *Green Energy Environ.* **2023**, *8*, 744–756. [[CrossRef](#)]
66. Renda, S.; Di Stasi, C.; Manya, J.J.; Palma, V. Biochar as support in catalytic CO₂ methanation: Enhancing effect of CeO₂ addition. *J. CO₂ Util.* **2021**, *53*, 101740. [[CrossRef](#)]
67. Santos, J.L.; Bobadilla, L.F.; Centeno, M.A.; Odriozola, J.A. Operando DRIFTS-MS Study of WGS and rWGS Reaction on Biochar-Based Pt Catalysts: The Promotional Effect of Na. *J. Carbon Res.* **2018**, *4*, 47. [[CrossRef](#)]
68. Wang, X.; Yang, M.; Zhu, X.; Zhu, L.; Wang, S. Experimental study and life cycle assessment of CO₂ methanation over biochar supported catalysts. *Appl. Energy* **2020**, *280*, 115919. [[CrossRef](#)]
69. Wang, X.; Liu, Y.; Zhu, L.; Li, Y.; Wang, K.; Qiu, K.; Tippayawong, N.; Aggarangsi, P.; Reubroycharoen, P.; Wang, S. Biomass derived N-doped biochar as efficient catalyst supports for CO₂ methanation. *J. CO₂ Util.* **2019**, *34*, 733–741. [[CrossRef](#)]
70. Di Stasi, C.; Renda, S.; Greco, G.; Gonzalez, B.; Palma, V.; Manya, J.J. Wheat-Straw-Derived Activated Biochar as a Renewable Support of Ni-CeO₂ Catalysts for CO₂ Methanation. *Sustainability* **2021**, *13*, 8939. [[CrossRef](#)]
71. Karimi, M.; Shirzad, M.; Silva, J.A.C.; Rodrigues, A.E. Biomass/Biochar carbon materials for CO₂ capture and sequestration by cyclic adsorption processes: A review and prospects for future directions. *J. CO₂ Util.* **2022**, *57*, 120592. [[CrossRef](#)]
72. Cao, L.; Zhang, X.; Xu, Y.; Xiang, W.; Wang, R.; Ding, F.; Hong, P.; Gao, B. Straw and wood based biochar for CO₂ capture: Adsorption performance and governing mechanisms. *Sep. Purif. Technol.* **2022**, *287*, 120592. [[CrossRef](#)]
73. Shafawi, A.N.; Mohamed, A.R.; Lahijani, P.; Mohammadi, M. Recent advances in developing engineered biochar for CO₂ capture: An insight into the biochar modification approaches. *J. Environ. Chem. Eng.* **2021**, *9*, 106869. [[CrossRef](#)]
74. Dekkar, S. Dry Reforming of Methane Over Ni/ZrO₂, Ni/CeO₂ and Ni/La₂O₃ Catalysts: Role of Support Nature and its Synthesis by Microemulsion Method. *Chem. Afr.* **2024**, *7*, 1–11. [[CrossRef](#)]

Disclaimer/Publisher's Note: The statements, opinions and data contained in all publications are solely those of the individual author(s) and contributor(s) and not of MDPI and/or the editor(s). MDPI and/or the editor(s) disclaim responsibility for any injury to people or property resulting from any ideas, methods, instructions or products referred to in the content.